Characterization of pulmonary arterial input impedance with lumped parameter models

BRYDON J. B. GRANT AND LINDA J. PARADOWSKI
Department of Medicine, State University of New York at Buffalo, Buffalo, New York 14215

GRANT, BRYDON J. B., AND LINDA J. PARADOWSKI. *Characterization of pulmonary arterial input impedance with lumped parameter models.* Am. J. Physiol. 252 (Heart Circ. Physiol. 21): H585–H593, 1987.—The purpose of this study is to evaluate systematically the ability of lumped parameter models to approximate pulmonary arterial input impedance (Z_{in}) and estimate characteristic impedance (Z_c) and pulmonary arterial compliance (C_{art}). To assess goodness of fit, the parameters of each model were adjusted so that the model's impedance approximates the Z_{in} measured in anesthetized cats. To assess the ability of the model to estimate Z_c and C_{art}, the lumped parameter models were fitted to Z_{in} calculated from a distributed parameter model of the feline pulmonary vasculature. In addition, we assessed the concordance between the lumped parameter model estimates of Z_c and C_{art}. The results indicate that no one model was superior; any of four models would be a reasonable choice. A four-element model was used to compare Z_{in} measured at different phases of the respiratory cycle. Small differences in the impedance spectra were found that have not been previously reported. We conclude that lumped parameter models can be used *1*) to provide close approximations to Z_{in}, *2*) to estimate Z_c and C_{art}, and *3*) to provide a useful approach for statistical comparisons of impedance spectra.

cats; characteristic impedance; pulmonary arterial compliance; mathematical models

PULMONARY ARTERIAL INPUT impedance is used as a descriptor of the right ventricular afterload (4). Because impedance is expressed in the form of moduli and phase angles as a function of frequency there have been attempts to present impedance data in a more concise form. The usual approach is to use a simple electrical network that has a similar impedance to pulmonary arterial input impedance. The parameter values of these electrical elements are used to provide an approximate description of the hemodynamic properties of the pulmonary vasculature. A number of these lumped parameter models have been developed, but there has been no systematic evaluation of their use. The purpose of this study is to find which of the electrical analogs is most appropriate to characterize pulmonary arterial input impedance.

The most appropriate model to represent pulmonary arterial input impedance may depend on the use of the model. Therefore, we used two criteria for testing these models: first, the adequacy of the impedance of the lumped parameter model to simulate the measured pulmonary arterial input impedance (goodness of fit), and second, the accuracy with which the lumped parameter model recovers values for characteristic impedance and total pulmonary arterial compliance calculated from a distributed parameter model of the pulmonary vasculature (numerical identification). We then tested the practical application of the lumped parameter models to experimental data.

METHODS

Lumped parameter models. Eight lumped parameter models are used in this study. There are between two and five elements in each model. The electrical analogs of these models are shown in Fig. 1. The simplest model (*model A*) is the two-element Windkessel which comprises of a resistor and capacitor in parallel (7). The resistor represents the viscous resistive properties of the pulmonary vasculature which are considered to reside primarily in the pulmonary microcirculation (3). The capacitor represents the compliant properties of the pulmonary arterial tree. All the other seven models are variations on this basic design.

Engleberg and Dubois (6) added an inductance in series with the Windkessel elements (*model B*). The inductance incorporates the inertial properties of the pulmonary vasculature due to the mass of blood. Westerhof and his colleagues (24) have used a different three-

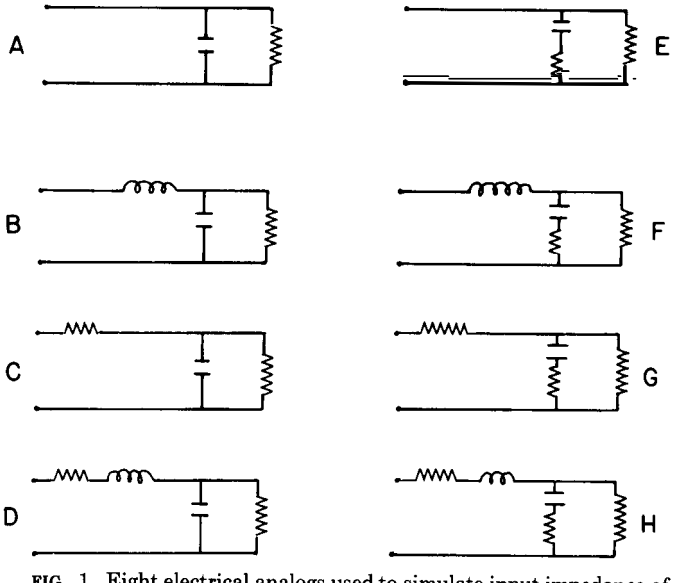

FIG. 1. Eight electrical analogs used to simulate input impedance of pulmonary vasculature.

element model in which the inductance is replaced by a resistor (*model C*). In this case the second resistor was used to reflect characteristic impedance. In a later version of this model (25) an inductance was introduced in series with this second resistor to produce a four-element model (*model D*). This element was used to permit positive phase angles in the impedance spectrum.

In all of these four models only the elastic properties of the vessel wall are expressed in terms of a capacitance. To include the viscous resistive properties of the vessel wall some investigators have used a Voigt viscoelastic element which consists of a resistor in series with the capacitance (21).

Models E–H were developed with this adjustment to *models A–D*, respectively. The relation between the eight models is shown in Fig. 2.

Method for testing goodness of fit. To test the ability of these lumped parameter models to fit experimental data, we measured pulmonary arterial input impedance in six cats that weighed between 2.5 and 5.0 kg. Anesthesia was induced with 20 mg/kg ketamine (Parke-Davis) intramuscularly and maintained with 0.67 ml/kg α-chloralose solution intravenously. The solution contains 60 mg/ml of α-chloralose (Sigma), 46 mg/ml of sodium tetraborate decahydrate (Sigma), and 25 mg/ml of sodium bicarbonate. Pancuronium bromide (Parke-Davis, 2 mg/kg iv) was used for muscular paralysis. The cats were ventilated through a tracheal cannula at 12–15 breaths/min and a tidal volume sufficient to maintain an arterial P_{CO_2} of 40 mmHg. A microswitch was added to the Harvard ventilator (model 618) to produce a 5-volt pulse at end-expiration. A femoral arterial catheter was placed for recording systemic blood pressure and obtaining blood samples to measure arterial blood gas composition (BMS 3 Mark 2 Blood microsystem). A femoral venous catheter was placed for additional injections of chloralose and pancuronium bromide as needed. After a midline thoracotomy, the pericardium was opened, and a Statham cuffed electromagnetic flow probe was placed around the main pulmonary artery. The flow probe was coupled to a Statham 2022 flowmeter with 100 Hz lowpass filter. We found that the flowmeter caused a phase shift of 1.8 degrees/Hz with no appreciable effect on amplitude (13).

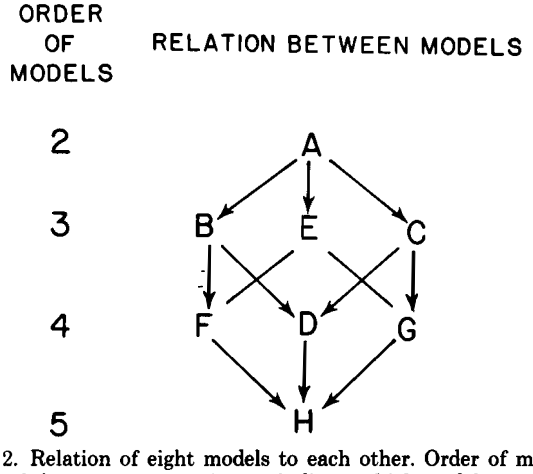

FIG. 2. Relation of eight models to each other. Order of model is number of elements present. *Arrows* indicate which models are nested. A nested model is a submodel of a higher order model. For example, all models are nested relative to *model H*, but *B, E,* and *C* are not nested, nor are *models F, D,* and *G*.

Pulmonary arterial pressure was measured by direct puncture of the pulmonary conus with a 0.8-mm Teflon catheter with its tip close to the cuffed flow probe. The catheter was connected to a Statham P23ID pressure transducer and flushed with degassed saline. The catheter transducer system has a resonant frequency of 73.0 Hz and a damping ratio of 0.109 as tested by a pop test (9). The electrocardiogram was monitored throughout the experiment and all electrical signals were recorded on an eight-channel Gould ink recorder and an eight-channel Hewlett-Packard FM tape recorder for further analysis. Pressure and flow data was digitized onto a North Star Horizon computer from the tape recorder at a tape speed of 3.75 in/s at a sampling rate of 333 Hz. Heart cycles were selected from 10 successive breaths: 10 cycles at end-expiration and 10 cycles end-inspiration which were identified from the output of the ventilator microswitch. The start and finish of individual heart cycles were identified from the QRS complex of the electrocardiogram. This approach divides each cardiac cycle in late diastole when there is minimal change of pulmonary arterial pressure and flow and avoids sharp discontinuities in the data that could cause "leakage" with Fourier analysis (4). The Fourier series of the pressure and flow signals for each cardiac cycle were corrected for the frequency response of the pressure and flow measurement systems. The inverse Fourier transform was performed, and the corrected pressure and flow signals were inspected to verify that the diacrotic notch of the pressure and flow signals were synchronized, which indicates that the pressure and flow are measured at the same site (23). Pulmonary arterial input impedance was calculated for 20 harmonics in polar form

$$Z(\omega) = P(\omega)/\dot{Q}(\omega) \quad (1)$$

$$Z(\omega) = A(\omega)e^{j\phi(\omega)} \quad (2)$$

where $Z(\omega)$ is the input impedance as a function of ω (angular frequency, rad/s), P and $\dot{Q}$ are the pressure and flow as functions of ω, respectively. $Z(\omega)$ is expressed in polar form in the complex plane. At each ω, there is a modulus, A, and a phase angle, ϕ. j is the square root of minus one. At each harmonic, the mean of the moduli of 10 cardiac cycles and the standard error of the mean were calculated. Calculation of the mean and confidence limits for the phase angle required the use of angular statistical methods (12). The standard deviation of the phase angle was estimated from Rayleigh's r statistic based on the normal circular distribution of von Mises (28). An advantage to this approach is that it provides an objective method of detecting higher harmonics where the noise is too great to be able to define a mean angle because the confidence limits increase without bound. If Rayleigh's r statistic indicates that 95% confidence limits could not be assigned to the phase angles of two successive harmonics, then those and higher harmonics were excluded from further analysis.

Fitting lumped parameter models to experimental data. Input impedance spectra are usually displayed in polar form. For the purpose of fitting impedance spectra of lumped parameter models to experimental data, the measured pulmonary arterial input impedance was expressed

in rectangular coordinate form rather than polar form

$$A(\omega)e^{j\phi(\omega)} = Z_R(\omega) + jZ_I(\omega) \quad (3)$$

where Z_R is the real component and Z_I is the complex component of impedance at a particular value of ω. At each harmonic the standard deviations (σ_R and σ_I) were calculated for Z_R and Z_I, respectively. To each set of impedance data, we optimized the parameters of the impedance of each of the eight-lumped parameter models with a Marquardt procedure (2). Since all eight models are nested in relation to *model H*, the impedance of each model can be derived from the impedance of *model H* by setting one or more parameters to zero. The impedance of *model H* ($Z_M(\omega)$) is

$$Z_M(\omega) = Z_{MR}(\omega) + jZ_{MI}(\omega) \quad (4)$$

$$Z_{MR}(\omega) = R_1 + [R_2 + \omega^2C^2R_2R_3(R_2 + R_3)]/ \quad (5)$$

$$(1 + \omega^2C^2R_2^2R_3^2) \quad (6)$$

$$Z_{MI}(\omega) = \omega L - \omega CR_2^2/[1 + \omega^2C^2(R_2 + R_3)^2]$$

Z_{MR} and Z_{MI} are the real and complex components of Z_M. R_1, R_2, L and C are values of the resistors, inductance, and capacitor, respectively, as indicated in Fig. 3. Estimates of the model parameters were obtained by minimizing the weighted residual sum of squares in the complex plane (WRSS). The residual sum of squares are weighted by experimental error according to the following equation

$$WRSS = \sum_{\omega=0}^{\omega=h} \{(1/\sigma_R^2)\,[Z_{MR}(\omega) - Z_R(\omega)]^2 + (1/\sigma_I^2)[Z_{MI}(\omega) - Z_I(\omega)]^2\} \quad (7)$$

where h is the angular frequency of the highest harmonic.

Assessment of model adequacy. Of the eight models, one has two parameters, three have three parameters, three have four parameters, and one has five parameters. For each data set we estimated the reduced chi-squared value (χ_v^2) for each model

$$\chi_v^2 = WRSS/df \quad (8)$$

where df represents the degrees of freedom ($N - P$).

The χ_v^2 is the ratio of the variance of the data points from the model's impedance to the variance of the measured data points due to experimental error. When χ_v^2 is less than unity, it indicates that the model's impedance is an adequate description of the data for the degree of experimental error. When χ_v^2 is greater than unity, it indicates that there are features of the measured impedance spectrum not described by the model.

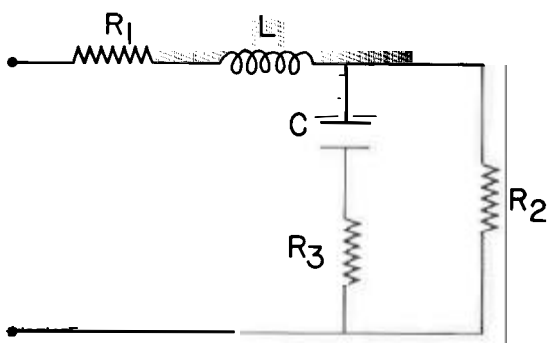

FIG. 3. Five-element *model H*. Diagram gives code for resistors (R_1 R_2, R_3), capacitance (C), and inductance (L).

To determine the most efficient model for fitting the data, we started with the lowest order model (*model A*) and determined if an additional parameter was justified by the reduction in the sum of squares with an F test (21)

$$F = [(WRSS_1 - WRSS_2)/(P_2 - P_1)]/[WRSS_2/(N - P_2)] \quad (9)$$

where N is the number of data points, P is the number of parameters in the model, and subscripts 1 and 2 refer to the lower and higher order models, respectively. Since there were three models each with three parameters, we selected the model from these three with the lowest residual sum of squares. Similarly we compared the best three-parameter model with the best four-parameter model, and the best four-parameter with the five-parameter model with an F test. Strictly, this approach can only be used for nested models (11). Therefore, we also used two other approaches to determine the model with the best fit: the Akaike information criterion (AIC) (1), and the Schwartz criterion (SC) (18)

$$AIC = WRSS + 2P \quad (10)$$

$$SC = WRSS + P \ln (N) \quad (11)$$

The best model is the one with the lowest values of AIC or SC.

Methods for testing numerical identification. To test the extent to which these lumped parameters represent physiological characteristics, we fitted the lumped parameter model to impedance spectra estimated from a distributed parameter model (27, 29). Instead of using impedance spectra measured experimentally, we used impedance spectra calculated from a distributed model of the pulmonary vasculature of the cat, because the true values of characteristic impedance and pulmonary arterial compliance can be estimated directly. These data (27, 29) provide the length, diameter, compliance, and number of branches of each order of the pulmonary vasculature and the length, surface area, and compliance of the pulmonary microcirculation. The intravascular pressure at each level in the pulmonary vasculature was calculated as described by Zhuarg et al. (29). The oscillatory pressure and flow were calculated with the Womersley equations as described by Weiner et al. (26). Details are provided in the APPENDIX. From this distributed parameter model we directly calculated pulmonary arterial input resistance (R_{in}), total pulmonary arterial compliance (C_{art}) and characteristic impedance (Z_C). Pulmonary arterial input resistance was defined as the mean pulmonary arterial pressure divided by mean pulmonary arterial flow, that is, the modulus of impedance at zero frequency. We varied the dimensions and elasticity of the pulmonary arterial tree to obtain eight impedance spectra with 10 harmonics of a fundamental frequency of 2.5 Hz similar to impedance spectra measured experimentally. The lumped parameter model was then fitted to the calculated impedance spectra. We compared the

true value of R_{in}, C_{art}, and Z_c with the values recovered with the lumped parameter model.

Assessment of numerical identification. To each input impedance from the distributed parameter model, we fitted the eight-lumped parameter models by the least squares approach outlined above without applying weights for experimental error. The residual sum of squares (RSS) was calculated from the following equation

$$RSS = \sum_{\omega=0}^{\omega=h} \{[Z_{MR}(\omega) - Z_R(\omega)]^2 + [Z_{MI}(\omega) - Z_I(\omega)]^2\}$$

Recovered parameter values were compared with R_{in}, C_{art}, and Z_c (see Table 1). The comparisons were assessed by linear regression analysis (20) with R_{in}, C_{art}, and Z_c considered as the independent variables. The primary test of numerical identification is Pearson's correlation coefficient, since this measure assessed the extent that the estimated R_{in}, C_{art}, and Z_c reflect changes of the true R_{in}, C_{art}, and Z_c. A secondary test of numerical identification is that of the regression equation. A regression coefficient of unity with a zero intercept would indicate perfect accuracy of recovered lumped parameter values.

Application of lumped parameter models. The practical application of lumped parameter models to experimental data was tested in two ways. First, to determine the concordance between the lumped parameter models for recovering characteristic impedance and pulmonary arterial compliance from impedance spectra measured experimentally. Second, to test the hypothesis that the pulmonary arterial input impedance does not vary during the respiratory cycle.

To determine the degree of concordance between the recovered values of Z_c and of C_{art} for the lumped parameter models, Kendall's coefficient of concordance (W) was calculated from the average value of Spearman's rank correlation coefficient (r_s) between all possible pairs of model determinations (19)

$$W = [r_s(k - 1) + 1]/k \quad (13)$$

where k is the number of models. To provide some indication of the relative degree of concordance for each model, we developed an index of concordance by calculating the Spearman's rank correlation coefficient for the recovered model values compared with the average value recovered by all models. This index is not used for statistical testing but merely to provide some qualitative comparison of the extent of concordance for each model.

To determine whether or not the pulmonary arterial input impedance varied during the respiratory cycle, we compared impedance measured at end-expiration with impedance measured at end-inspiration in each of the six cats. We used the same lumped parameter model to fit each pair of impedance spectra (*model F*). The WRSS was estimated for each spectrum, but deviations from the zero harmonic term were ignored. WRSS for each spectrum was summed (WRSSs) and compared with the WRSS from pooled data (WRSSp) using the F test

$$F = \left[\sum_{i=1}^{i=D} \{WRSSp - WRSSs\}/(D \cdot P)\right] \Big/ \left[\sum_{i=1}^{i=D} WRSSs/(D\{N - P\})\right] \quad (14)$$

where D is the number of pairs of impedance spectra to be compared, and N is the sum of the number of harmonics used in each spectrum.

TABLE 1. *Numerical identification with lumped parameter models*

Model	Elements	Representation	
		R_{in}	Z_c
A	$R_2\,C$	R_2	
B	$L\,R_2\,C$	R_2	$(L/C)^{1/2}$
C	$R_1\,R_2\,C$	$R_1 + R_2$	R_1
D	$R_1\,L\,R_2\,C$	$R_1 + R_2$	R_1
E	$R_2\,C\,R_3$	R_2	R_3
F	$R_2\,L\,C\,R_3$	R_2	R_3
G	$R_1\,R_2\,C\,R_3$	$R_1 + R_2$	$R_1 + R_3$
H	$R_1\,L\,R_2\,C\,R_3$	$R_1 + R_2$	$R_1 + R_3$

R_{in} is pulmonary arterial input resistance (mean pulmonary arterial pressure divided by mean flow); Z_c is characteristic impedance. Representation of compliance is the capacitance C for all models. L, inductance.

RESULTS

An example of the pulmonary arterial input impedance (Z_{in}) that was measured experimentally and of the impedance generated from the distributed parameter model are shown in Fig. 4. Some of the impedance spectra generated by the distributed parameter model exhibited marked fluctuations of the moduli at higher frequencies of the spectrum compared with the pulmonary arterial input impedance measured experimentally. Nevertheless, the spectra are fairly similar. The marked fluctuations of moduli in impedance spectra generated by the distributed parameter model are probably due to the symmetrical nature of the system (21).

Goodness of fit to experimental data. To test the adequacy of fit we used χ^2_v test. By this criterion we found that *models C–H* provide adequate fits to the experimental data for 6 out of the 12 impedance spectra, since χ^2_v was less than unity. For the six spectra that were not described adequately by the lumped parameter models, we determined the maximal χ^2_v that each model produced. *Models D* and *F* had the lowest maximal χ^2_v, which indicates that they provided the closest fits to the experimental data under the most adverse conditions.

Three criteria were used to assess the goodness of fit of the lumped parameter models to the experiment data: the F test, the Akaike information criterion, and the Schwartz criterion. Regardless of the criteria used, the same four models (C–F) stand out as being superior (Fig. 5).

Numerical identification from distributed parameter model. Of the eight models, six provided strong correlations between the actual and recovered values of characteristic impedance from the distributed parameter model (Fig. 6). Only two models (*A* and *B*) did not provide reasonable values of characteristic impedance. There were few parameters in *model A*, and the values for Z_c in *model B* were all close to zero. The regression coefficients

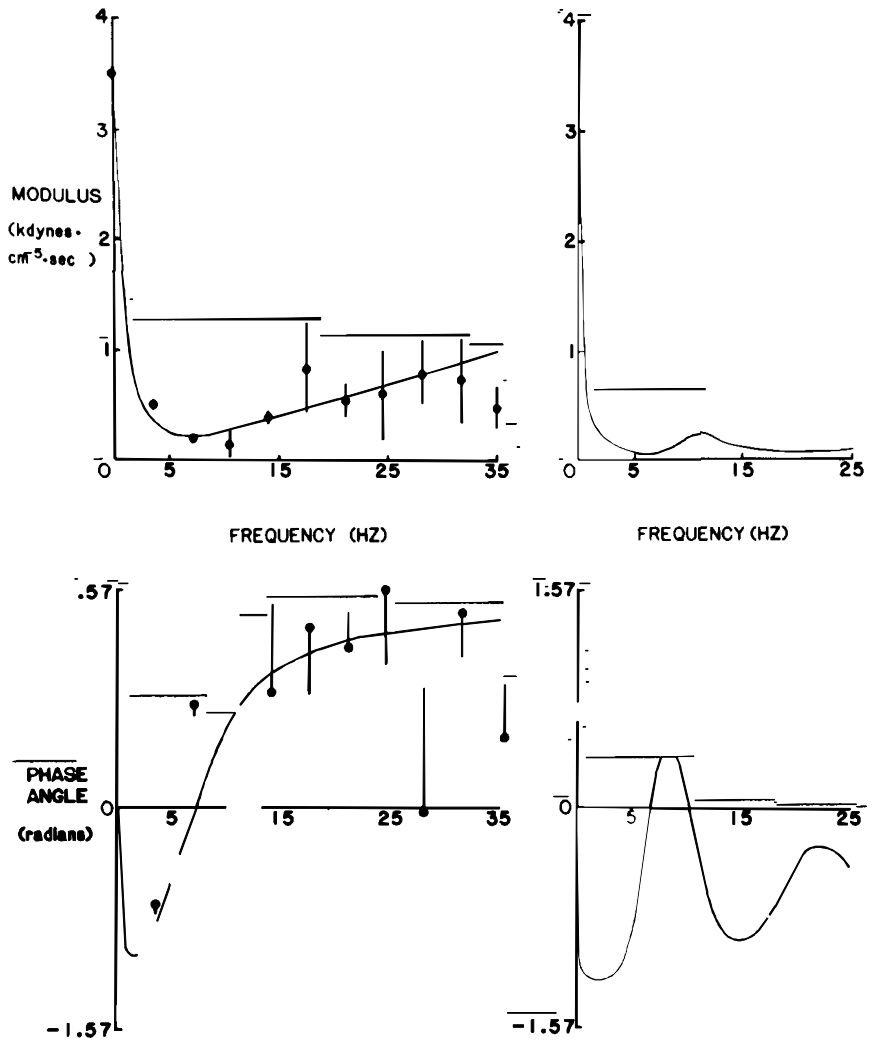

FIG. 4. Examples of pulmonary arterial input impedance measured by experiment (*left*) and calculated from distributed parameter model (*right*) with same input values used by Zhuarg et al. (29). *Top panels* show moduli (*ordinates*) and *bottom panels* show phase angles (*ordinates*). Both are plotted against frequency (Hz). *Bars* on measured impedance data indicate two standard errors of mean for moduli and 95% confidence limits for phase angles.

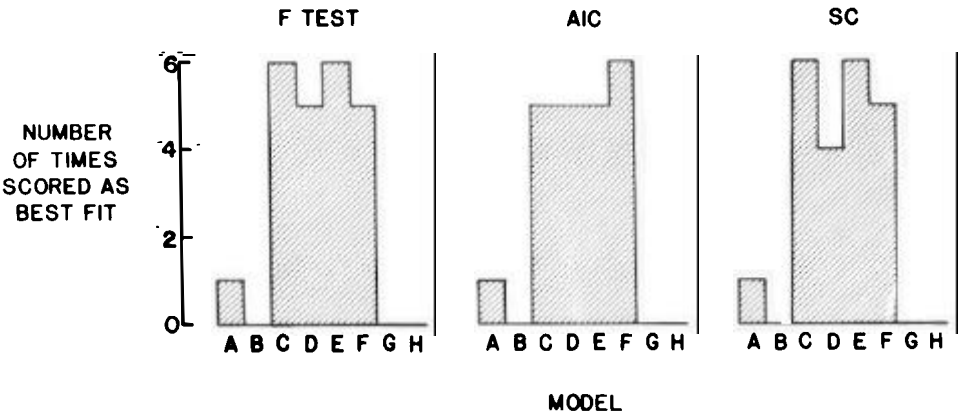

FIG. 5. Goodness of fit assessed by variance ratio (F test), Akaike information criterion (AIC), and Schwartz criterion (SC). Each *histogram* indicates number of times a particular model scores as a best fit for 12 measured pulmonary arterial input impedance spectra. In most cases there are ties for best fit.

were higher than unity (Table 2) mainly due to overestimates of Z_c for two data sets when characteristic impedance was high.

All eight models provided good correlations between the actual and recovered values of arterial compliance. The simplest model (*model A*) provided the best correlation coefficient (Fig. 7) but not the best regression coefficient (Table 2) largely due to underestimating low compliance values (Fig. 8).

Practical application of lumped parameter models to experimental data. When the models were used to determine the characteristic impedance from the experimental data, there was nearly perfect agreement among all six models (*C–F*). The W was 0.975. Not surprisingly, the index of concordance was equally high for all six models (Fig. 9). Therefore, the choice of model had little effect on the estimate of Z_c from experimental data. This agreement between models was not so close for the determination of arterial compliance: the coefficient of concordance was only 0.75. For C_{art}, the index of concordance was similar for seven of the eight models; only *model B* produced results that differed substantially from

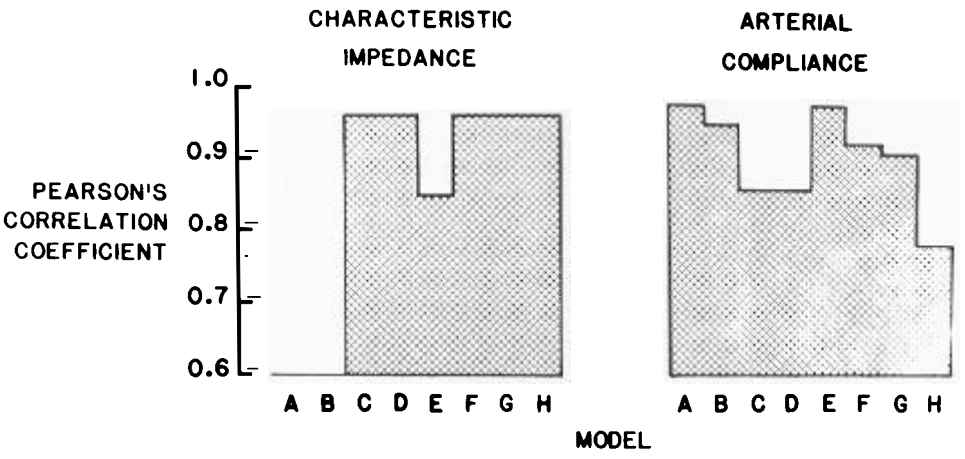

FIG. 6. Numerical identification of characteristic impedance (Z_c) and total pulmonary arterial compliance (C_{art}) in distributed model. *Histograms* compared Pearson's correlation coefficients for each of 8 models. True values of each parameter (Z_c and C_{art}) from distributed parameter model are correlated with values recovered from its impedance spectra with lumped parameter model.

TABLE 2. *Numerical identification of pulmonary arterial compliance and characteristic impedance*

Model	Arterial Compliance			Characteristic Impedance		
	Correlation coefficient	Regression coefficient	Constant term	Correlation coefficient	Regression coefficient	Constant term
A	0.975	1.288	−0.095	NA	NA	NA
B	0.947	1.197	−0.039	NA	NA	NA
C	0.866	1.033	0.022	0.963	1.413	−0.093
D	0.863	1.166	0.031	0.962	1.423	−0.095
E	0.970	1.259	−0.084	0.854	1.450	−0.077
F	0.926	1.393	−0.062	0.959	2.056	−0.204
G	0.916	1.143	−0.019	0.96	1.482	−0.10
H	0.787	1.065	0.037	0.958	1.501	−0.103

NA, model is not capable of identifying approximate values of characteristic impedance.

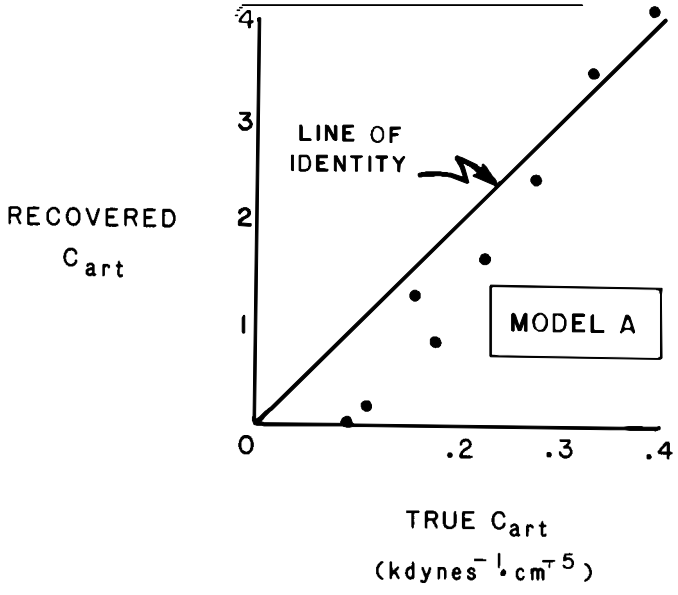

FIG. 7. Correlation between true values of pulmonary arterial compliance in distributed parameter model (*abscissa*, true C_{art}) and values recovered from its impedance spectra with lumped parameter *model A* (*ordinate*, recovered C_{art}). Correlation coefficient is 0.975.

the others (Fig. 9).

We used the lumped parameter *model F* to test for differences in the impedance spectra measured at end-expiration and end-inspiration. We found that there was a significant difference between the spectra ($F = 1.62$, $P < 0.05$). When individual experiments were analyzed with the F test using the Bonferroni adjustment only one experiment showed a significant difference of Z_{in} between end-expiration and end-inspiration (Fig. 10). Neither of the model values of Z_c or C_{art} showed significant differences between end-expiration and end-inspiration; Z_c was 0.31 ± 0.11 and 0.23 ± 0.05 kdyn·s^{-1}·cm^{-5} (SE), respectively, C_{art} was 0.13 ± 0.02 and 0.14 ± 0.02 kdyn^{-1}·cm^{+5} (SE), respectively. Nevertheless there is a significant positive correlation between change in mean pulmonary arterial pressure from end-expiration to end-inspiration with the F value for each experiment ($r = 0.76$, $P < 0.05$, $n = 6$). The F value is a measure of the difference between impedance spectra. This result suggests that the extent to which the impedance spectrum varies during the respiratory cycle depends on the change of the mean pulmonary arterial pressure during the respiratory cycle.

DISCUSSION

Comparison of lumped parameter models. Even the most cursory inspection of the results would indicate that there is little basis to choose between four models (*C–F*); each of the other four models have at least one drawback. *Models A* and *B* do not fit the impedance data well, and *models G* and *H* contain elements that do not contribute significantly to the ability of the model to fit the data. Furthermore, *models A* and *B* do not contain elements that can be used to estimate characteristic impedance. From this perspective *model B* is somewhat disappointing because it contains an inductance and a capacitance which is potentially a more realistic approach to simulating characteristic impedance than the resistor used in *models C* and *F*. On the other hand these four models (*A, B, G,* and *H*) are not entirely devoid of merit. For example, *model A* is particularly good for estimating pulmonary arterial compliance from impedance spectra generated from the distributed parameter model. Paradoxically, this result may be due to the inability of the model to fit the data well. As a result the model tends to average the fluctuations of the moduli and phase angles with frequency due to wave reflection.

Adequacy of fit. In the real system wave reflection has less effect on input impedance. Consequently good fits of the experimental data are obtained with lumped parameter models. The ability of lumped parameter models to fit the experimental data can be gauged from the χ^2_ν (see *Eq. 8*). Six of the 8 models provided adequate fits to

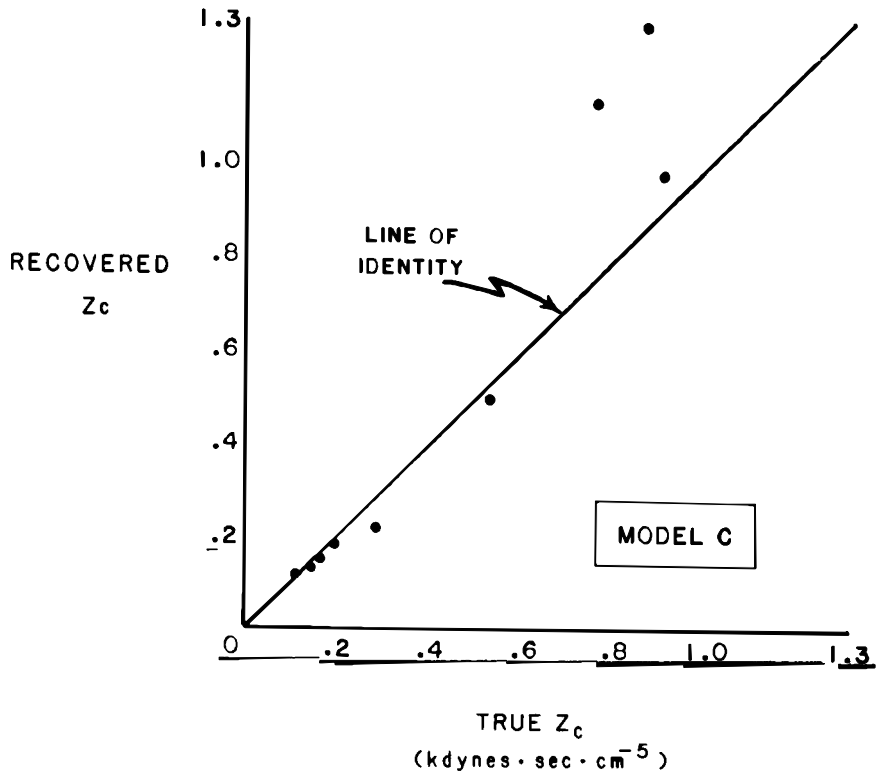

FIG. 8. Correlation between true values of characteristic impedance (Z_c) in distributed parameter model (*abscissa*, true Z_c) and values recovered from its impedance spectra with lumped parameter *model C* (*ordinate*, recovered Z_c). Correlation coefficient is 0.963.

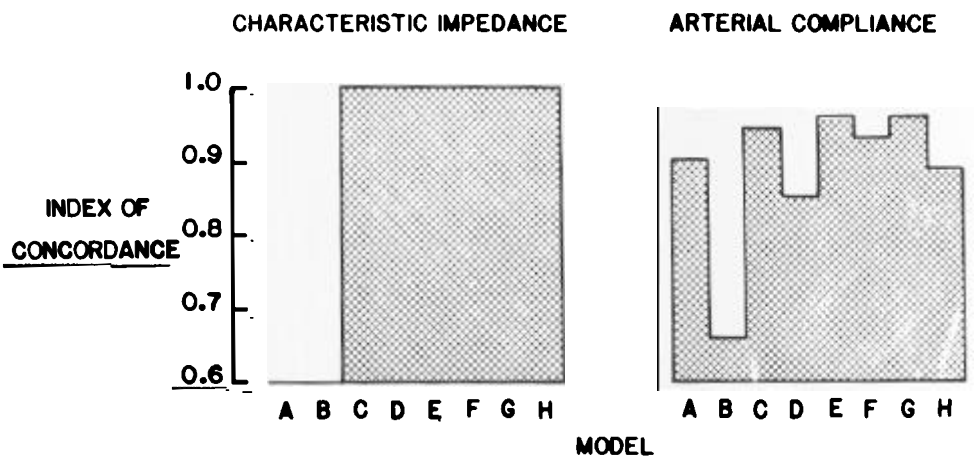

FIG. 9. Histogram of degree of concordance of recovered value. Index of concordance was obtained by calculating Spearman's rank correlation coefficient for recovered value of each parameter (characteristic impedance or arterial compliance) with average value recovered by all 8 models.

6 of the 12 measured impedance spectra by this criterion. Adequacy of fit by the reduced chi-squared criterion indicates that deviations of the experimental data from the model impedance spectrum can be accounted for entirely by experimental errors.

Limitations. It should be emphasized that this study is limited to the application of lumped parameter models to pulmonary arterial input impedance. No attempt is made in this paper to determine the most accurate way of measuring pulmonary arterial input impedance, characteristic impedance, or pulmonary arterial compliance. Nevertheless the results do suggest that the lumped parameter models are capable of providing approximate estimates of these parameters. In addition, it should be mentioned that the use of lumped parameter models to compare impedance spectra is not necessarily the most efficient approach. If the impedance spectra are obtained at a constant fundamental frequency by pacing the heart for example, then the impedance spectra can be compared by analysis of variance with a nested design without the need to invoke regression techniques. The advantage of the lumped parameter model approach is that it does not require the impedance moduli and phase angles to be measured at the same frequencies to permit comparisons.

Impedance changes during respiratory cycle. We used the lumped parameter model to test for differences in pulmonary input impedance during the respiratory cycle. Changes of pulmonary arterial input impedance during the respiratory cycle have not been previously reported. We found differences in the impedance spectra measured at end-expiration and at end-inspiration, but we did not find any difference in C_{art}. Z_c tended to be larger at end-expiration, but this difference was not significant. This difference in the impedance spectra might seem unimportant, since only one of the six experiments showed a significant difference when each experiment was analyzed individually. Nevertheless the fact that the F value

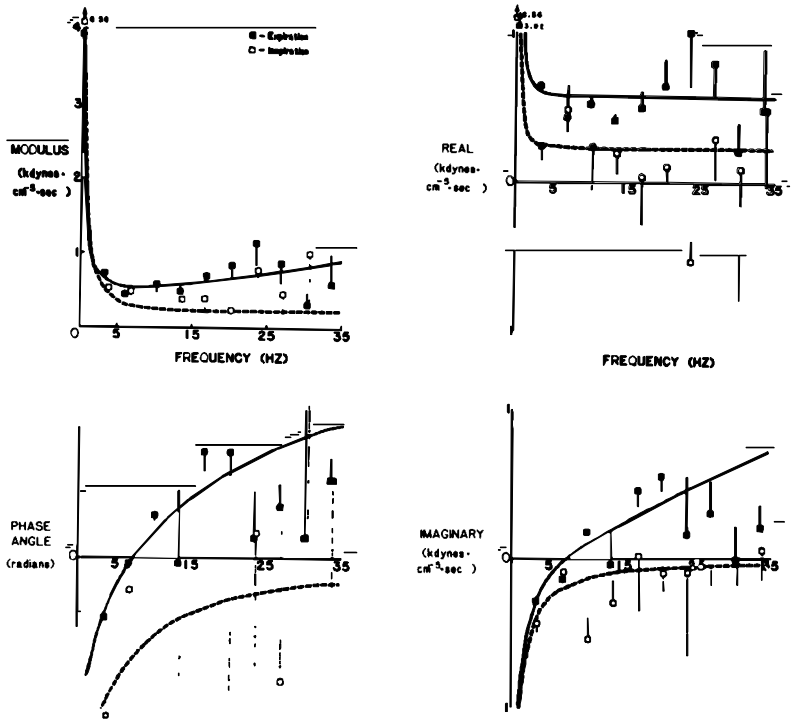

FIG. 10. Comparison of pulmonary arterial input impedance obtained at end-expiration (*closed squares continuous line*) with impedance obtained at end-inspiration (*open squares interrupted line*). *Top panel* shows moduli (*ordinate*) and *bottom panel* phase angles (*ordinate*); both are plotted against frequency (*abscissa*). *Bars* indicate two standard errors of mean for moduli and 95% confidence limits for phase angles. Data are from experiment that showed greatest variation of impedance with respiration.

correlated with the difference in mean pulmonary arterial pressure between end-expiration and end-inspiration suggests this finding does have a physiological basis. Clearly, further studies would be needed to investigate this matter. The point that should be emphasized is that this statistical approach is a powerful means of detecting differences between impedance spectra.

Practical application of lumped parameter models. The reasons for using lumped parameter models to describe pulmonary arterial input impedance are fourfold: *1*) to provide a simple description of the spectrum (for example see Ref. 16), *2*) to use the spectra generated from lumped parameter models in mathematical models of right ventricular-vascular interaction (for example see Ref. 17), *3*) to estimate characteristic impedance and pulmonary arterial compliance (for example see Ref. 22), *4*) to compare impedance spectra (for example see Ref. 5, 11, 19). If one model was to be selected, then *model F* is probably the best overall choice. We reached this conclusion for the following reasons. First, it is one of the four models (*C–F*) that best fit the data, and second, it provides reasonable estimates of characteristic impedance and arterial compliance. The fact that it has four instead of three elements means that for some impedance spectra the inductance is superfluous. Inclusion of the inductance does not have a deleterious effect on parameter estimation, because in these circumstances it is optimized to a value close to zero. The only penalty is the loss of a degree of freedom. This penalty is offset by the fact that other spectra do require the inductance to describe the positive phase angles in the impedance spectrum. Nevertheless, any of the four models including the commonly used *models C* and *D* are all reasonable alternatives. The choice of model will depend on the purpose for which it is used.

APPENDIX

Distributed parameter model

The data of Zhuarg et al. (29) gives the length, diameter, apparent viscosity of blood, compliance, and number of branches at each order of the pulmonary vasculature. Because the diameter of each order is dependent on the intravascular pressure, we calculated the mean pressure at the entrance and exit at each order of the arteries and veins according to the fifth power law (29). Changes in pressure at the junctions of each order of the pulmonary vasculature from the left atrium to the main pulmonary artery due to the Bernoulli effect were taken into account in a manner described by Zhuarg et al. (29). For the pulmonary capillary sheet we subdivided it along its length into 31 units and applied sheet-flow equations to calculate entrance and exit pressures for each unit. Thus a series of linear approximations was used to overcome the nonlinearities of the sheet. For oscillatory flow we defined the longitudinal (Z_L) and transverse impedance (Z_T) for each order

$$Z_L = -(dP/dx)/Q = R + L(dQ/dt)/Q \qquad (15)$$

$$Z_T = -P/(dQ/dx) = -P/C(dP/dt) \qquad (16)$$

where P is pressure, Q is flow in the axial direction, x is axial length, R is resistance per unit length, C is compliance per unit length, and L is inertance per unit length. From the telegraph line equations it can be shown that characteristic impedance (Z_c) is

$$Z_c = [Z_L/Z_T]^{1/2} = [(R + j\omega L)/j\omega C]^{1/2} \qquad (17)$$

where Z_L and Z_T have been expressed in the frequency domain so that j is the square root of minus one, and ω is the angular frequency expressed as radians per second. Similarly, we estimate the propagation coefficient (γ) as

$$\gamma = [Z_L \cdot Z_T]^{1/2} = [(R + j\omega L)j\omega C]^{1/2} \qquad (18)$$

To calculate Z_c and γ as functions of ω we need to calculate R,

L, and C. R and L were calculated from the equations

$$R = [4\ \rho\omega/(\pi D^2 M)]\sin\theta \quad (19)$$

$$L = [4\ \rho/(\pi D^2 M)]\cos\theta \quad (20)$$

where ρ is the density of blood, D is the vessel diameter which is an average of diameter at the entrance and exit of the vessel, M and θ have numerical values that are tabulated by Womersley as functions of the dimensionless parameter α which is defined as

$$\alpha = (D/2)(\rho\omega/\mu)^{1/2} \quad (21)$$

where μ is apparent blood viscosity. The exact values of M and θ for a given α were derived by interpolation of the tabulated values (16). For small values of ω, θ tends to 90 degrees and α^2/M tends to 8 degrees. Zhuarg et al. (29) defined compliance as (dD/dP). In the equations for Z_c and γ, compliance is defined as (dV/dP) per unit length where V is the volume of the vessel. Wall thickness is assumed to be negligible in relation to the diameter. To convert compliance into this form we used the identity

$$dV/dP = (dD/dP)(dV/dD) \quad (22)$$

where $dV/dD = \pi DL/2$ and L is the length of the vessel.

After calculation of Z_c and γ the next step is to calculate the reflection coefficient (Γ)

$$\Gamma = (Z_T - Z_c)/(Z_T + Z_c) \quad (23)$$

We started at the point where the pulmonary veins exit into the left atrium. The left atrium is assumed to act like an open reservoir so the input impedance at this point has a modulus of zero and a phase angle of 90 degrees at all nonzero frequencies. We then worked backwards along each order of the pulmonary vasculature from the left atrium to the main pulmonary artery. At each level we calculated the input impedance (Z_i) at the entrance to a vessel of that order

$$Z_i = Z_c[1 + \Gamma\exp(-2\gamma 1)]/[1 - \Gamma\exp(-2\gamma 1)] \quad (24)$$

We used a symmetrical model of the pulmonary vasculature so that the total input impedance at the entrance of an order of the pulmonary vasculature can be estimated from Z_i/n, where Z_i is the input impedance of a vessel of that order, and n is the number of branches of the order.

We thank Drs. Robert E. Mates and John M. Canty for useful discussions, Marsha Barber for typing the manuscript, and Steven Neth and Pamela Krawcyzk for expert technical assistance.

This work was supported in part by a grant-in-aid from the American Heart Association and West Palm Beach Chapter of the American Heart Association, and a grant from the Whitaker Foundation. B. J. B. Grant is a recipient of Research Career Development Award HL-01418 from National Heart, Lung, and Blood Institute.

Received 10 March 1986; accepted in final form 24 October 1986.

REFERENCES

1. AKAIKE, H. A new look at the statistical model identification. *IEEE Trans. Autom. Control* AC19: 716–723, 1974.
2. BEVINGTON, P. R. *Data Reduction and Error Analysis for the Physical Sciences.* New York: McGraw Hill, 1969.
3. BHATTACHARYA, J., AND N. C. STAUB. Direct measurement of microvascular pressures in the isolated perfused dog lung. *Science Wash. DC.* 210: 327–328, 1980.
4. BRIGHAM, E. O. *The Fast Fourier Transform.* Englewood Cliffs, NJ: Prentice-Hall, 1974.
5. CALVIN, JR., J. E., R. E. BAER, AND S. A. GLANTZ. Pulmonary artery constriction produces a greater right ventricular dynamic afterload than lung microvascular injury in the open chest dog. *Circ. Res.* 56: 40–56, 1985.
6. ENGLEBERG, J., AND A. B. DUBOIS. Mechanics of pulmonary circulation in isolated rabbit lungs. *Am. J. Physiol.* 196: 401–414, 1959.
7. FRANK, O. Die Grandform des arteriellen Pulses. Erste Abhandlung mathematische Analyse. *Z. Biol.* 37: 483–526, 1899.
8. FUNG, Y. C. Theoretical pulmonary microvascular impedance. *Ann. Biomed. Eng.* 1: 221–245, 1972.
9. GABE, I. T. Pressure measurement in experimental physiology. In: *Cardiovascular Fluid Dynamics,* edited by D. H. Bergel, London: Academic, 1972, Vol. 1, p. 11–50.
10. HOPKINS, R. A., J. W. HAMMON, JR., P. A. MCHALE, P. K. SMITH, AND R. W. ANDERSON. An analysis of the pulsatile hemodynamic responses of the pulmonary circulation to acute and chronic pulmonary venous hypertension in the awake dog. *Circ. Res.* 47: 902–910, 1980.
11. LANDAW, E. M., AND J. J. DISTEFANO III. Multiexponential, multicompartmental and noncompartmental modeling. II. Data analysis and statistical considerations. *Am. J. Physiol.* 246 (*Regulatory Integrative Comp. Physiol.* 15): R665–R677, 1984.
12. MARDIA, K. V. *Statistics of Directional Data.* New York: Academic, 1972.
13. MILLS, C. H. Measurement of pulsatile flow and flow velocity. In: *Cardiovascular Fluid Dynamics,* edited by D. H. Bergel, London: Academic, 1972, Vol. 1, p. 51–90.
14. MILNOR, W. R. Arterial impedance as ventricular afterload. *Circ. Res.* 36: 565–570, 1975.
15. MILNOR, W. R. *Hemodynamics.* Baltimore, MD: Williams and Wilkins, 1982.
16. PIENE, H. Some physical properties of the pulmonary arterial bed deduced from pulmonary arterial flow and pressure. *Acta Physiol. Scand.* 98: 295–306, 1976.
17. PIENE, H., AND T. SUND. Does normal pulmonary impedance constitute the optimum load for the right ventricle? *Am. J. Physiol.* 242 (*Heart Circ. Physiol.* 11): H154–H160, 1982.
18. SCHWARTZ, G. Estimating the dimension of a model. *Am. Stat.* 6: 461–464, 1978.
19. SEIGEL, S. *Nonparametric Statistical Methods for the Behavioral Sciences.* Kogakusha, McGraw-Hill, 1956.
20. SNEDECOR, G. W. AND W. G. COCHRAN. *Statistical Methods* (6th ed). Ames: Iowa State Univ. Press, 1967.
21. TAYLOR, M. G. The input impedance of an assembly of randomly branching elastic tubes. *Biophysical J.* 6: 29–51, 1966.
22. VAN DEN BOS, G. C., N. WESTERHOF, AND O. S. RANDALL. Pulse wave reflection: can it explain the differences between systemic and pulmonary pressure and flow waves. *Circ. Res.* 51: 497–485, 1982.
23. WESTERHOF, J., G. ELZINGA, AND P. SIPKEMA. An artificial arterial system for pumping hearts. *J. Appl. Physiol.* 31: 776–781, 1971.
24. WESTERHOF, N., AND A. NOORDERGRAF. Errors in the measurement of hydraulic input impedance. *J. Biomech.* 3: 351–356, 1970.
25. WESTERHOF, J., G. ELZINGA, P. SIPKEMA, AND G. C. VAN DEN BOS. Quantitative analysis of the arterial system and heart by means of pressure-flow relations. In: *Cardiovascular Flow Dynamics and Measurements.* edited by N. H. C. Hwang and N. A. Normann. Baltimore, MD: University Park, 1977, p. 408–438.
26. WIENER, F., E. MORKIN, R. SKALAK, AND A. P. FISHMAN. Wave propagation in the pulmonary circulation. *Circ. Res.* 19: 834–850, 1966.
27. YEN, R. T., Y. C. FUNG, AND N. BRIGHAM. Elasticity of small pulmonary arteries in the cat. *J. Biomech. Eng.* 102: 170–177, 1980.
28. ZAR, J. H. *Biostatistical Analysis.* Englewood Cliffs, NJ: Prentice-Hall 1974.
29. ZHUARG, F. Y., Y. C. FUNG, AND R. T. YEN. Analysis of blood flow in cat's lung with detailed anatomic and elasticity data. *J. Appl. Physiol.* 55: 1341–1348, 1983.